Analyst

Accepted Manuscript

This article can be cited before page numbers have been issued, to do this please use: D. Wu, H. Zhang, D. Jin, Y. Yu, D. Pang, M. Xiao, Z. Zhang, Z. Zhang and G. Zhang, *Analyst*, 2019, DOI: 10.1039/C9AN01332F.

ROYAL SOCIETY OF CHEMISTRY

rsc.li/analyst

View Article Online
DOI: 10.1039/C9AN01332F

Microvesicles Detection by Reduced Graphene Oxide Field Effect Transistor Biosensor Based on a Membrane Biotinylation Strategy

Ding Wu[a, ξ], Hong Zhang[b, ξ], Dan Jin[a], Yi Yu[a], Dai-Wen Pang[c], Meng-Meng Xiao[d], Zhi-Ling Zhang[c,*], Zhi-Yong Zhang[d,*], Guo-Jun Zhang[a,*]

[a]School of Laboratory Medicine, Hubei University of Chinese Medicine, 16 Huangjia Lake West Road, Wuhan 430065, P.R. China

[b]Teaching and Research Office of Forensic Medicine, Hubei University of Chinese Medicine, 1 Huangjia Lake West Road, Wuhan 430065, P.R.China

[c]Key Laboratory of Analytical Chemistry for Biology and Medicine (Ministry of Education), College of Chemistry and Molecular Sciences, Wuhan University, Wuhan 430072, P.R.China

[d]Hunan Institute of Advanced Sensing and Information Technology, Xiangtan University, Hunan 411105, P. R. China

[ξ]These authors contributed equally to this work

[*]Corresponding author: Tel: +86-27-68890259, Fax: +86-27-68890259

E-mail: zhanggj@hbtcm.edu.cn, zlzhang@whu.edu.cn, zyzhang@pku.edu.cn

View Article Online
DOI: 10.1039/C9AN01332F

ABSTRACT

Unlike other extracellular-vesicles (EVs) subtypes such as exosomes, the lack of well-defined universal markers on the surface of microvesicles (MVs) has led to difficult detection of the entire MVs population. To design a universal MVs detection method, we report a highly sensitive electrical detection of MVs using a reduced graphene oxide (RGO) based field effect transistor (FET) biosensor by introduction of a membrane biotinylation strategy in this work. The biotinylated MVs (B-MVs) were obtained by supplying the culture medium with 1,2-distearoyl-sn-glycero-3-phosphoethanolamine-N-[biotinyl(polyethylene glycol)-2-000)] (DSPE-PEG-Biotin) while cultivating cells. An excellent biotinylation efficiency of B-MVs (92.6%) was then realized. Streptavidin (SA) probe was subsquently modified onto the channel surface of the as-fabricated RGO FET device, which was capable of specifically recognizing B-MVs due to the high affinity between SA and biotin in a 1:4 recognition format. The results showed that the RGO-based FET biosensor could detect B-MVs in a wide range from 10^5 particles/mL to 10^9 particles/mL with a low detection limit down to 20 particles/μL, which was the lowest compared with other reports. Such a platform also allowed for distinguishing the B-MVs from other unbiotinylated EVs types such as MVs and exosomes, exhibiting cracking specificity. Moreover, this FET biosensor demonstrated the capability of detecting B-MVs derived from different cell lines including cancer cells and normal cells, indicating its versatility and potential application in biomedical field.

KEYWORDS: Field effect transistor; biosensor; Reduced graphene oxide; Microvesicles detection; Cancer cell; Biotinylation

View Article Online
DOI: 10.1039/C9AN01332F

1. Introduction

Microvesicles (MVs) are a subgroup of extracellular vesicles with a diameter of 100-1000 nm, which are directly budding from cell membranes during cell activation or apoptosis.[1,2] MVs can present in different biological matrices, like cell culture supernatants, blood, hydrothorax and ascites, etc.[3,4] The membrane surface of MVs is highly inherited from maternal cell-specific receptors and antigens and can be recognized and ingested by specific recipient cells.[5] As known, MVs are a new type of messenger because almost all cells release MVs to communicate with other specific recipient cells, including cancer cells, endothelial cells, platelets, etc.[3,4] Hence, it is essential for us to analyze the overall level of MVs prior to clinical applications. Additionally, development of an analytical method to the entire MVs population provides us a completely new way to understand diverse cellular processes such as intracellular and intercellular communication (including transport, delivery, receptor-mediated signal transduction, etc) from a holistic perspective.[6] Moreover, the potential modulation mechanisms for MVs formation and elimination may be further interpreted by the analysis of overall level of MVs,[6-8] which can help us deeply understand the pathogenesis of various diseases with abnormal MVs concentrations, such as cardiovascular diseases,[9] autoimmune diseases,[10] neurological disorders[11] and various cancers[12-16] from a new perspective. More importantly, the detection for the entire MVs population can be employed as unique "bio-fingerprints" for many diseases.[14,16] Therefore, it is desirable to develop a highly sensitive and effective detection platform for the entire MVs population because of the special physicochemical properties of MVs, such as small particle size, "fragile" membrane structure.

Currently, the most routin MVs detection assays are primarily performed by

View Article Online
DOI: 10.1039/C9AN01332F

using flow cytometry (FCM), dynamic light scattering (DLS), nanoparticle tracking analysis (NTA), tunable resistive pulse sensing (TRPS) and enzyme-linked immunosorbent assay (ELISA), etc.[17-20] However, most of these assays suffer from those disadvantages, such as low sensitivity, high test cost, time and sample consuming and expensive instruments, which hamper their clinical applications. Fluorescence assay is also a widely used approach for detecting MVs. Chaudhuri et al.[21] reported the fluorescence detection of $CD45^+$ MVs through the anti-CD45 antibody functionalized microtubules. Nevertheless, they only reported a proof-of-principle platform to qualitatively detect MVs. Moreover, the detection of MVs was highly dependent on expensive and non-portable fluorescent imaging equipment. Fortunately, some breakthrough efforts have been made to detect MVs with portable devices in recent years, such as various well-designed biosensors to specifically detect MVs by the cell-specific markers on their surface. Cherré et al.[22] reported the specific capture of $CD31^+$ MVs derived from endothelial cell through anti-CD31 antibody immobilized on the magnetoresistive biosensor. Kailashiya et al.[23] developed an electrochemical biosensors for analyzing MVs derived from platelets through the anti-PAC1 antibody modified on the glassy carbon electrodes. Singh et al.[24] also demonstrated an electrochemical biosensor for MVs detection through anti-PAC1 and anti-P-selectin antibodies functionlized on the indium tin oxide (ITO) glass working electrode. Despite being promising platforms, most of them can only detect MVs derived from particular cell sources or platelet and are highly dependent on the expression of sufficient markers on their surface. Moreover,

View Article Online
DOI: 10.1039/C9AN01332F

the sensitivities of these assays are partly still not conductive to detect MVs in heterogeneous clinical samples with a low concentration. Therefore, there is a lack of well-designed biosensor to detect the entire MVs population due to the absence of well-defined universal markers on the surface of MVs. Compared to the assays mentioned above, the reduced graphene oxide (RGO) based Field-effect transistor (FET) biosensor provides a new method for detecting MVs with high sensitivity and specificity due to its inherent amplification capability and excellent conductivity of graphene.[25] Furthermore, the manufactured RGO-based FET biosensor has the following superiorities, such as low test cost, simple biosensor fabrication, low reagent and sample consumption (10 μL) and easy surface engineering, etc.[25] In our previous works, we have successfully appiled FET biosensors to detect various molecules such as proteins, nucleic acid, small molecules, etc.[25-31]

Herein, as diagrammed in Fig. 1, by introducing a membrane biotinylation strategy and a RGO-based FET biosensor, a high sensitivity, specificity and versatility detection method for MVs is proposed. To our knowledge, this is the first case of MVs detection using the FET biosensor. In order to establish a universal MVs detection method, we modify the MVs with biotin by supplying the cell culture medium with DSPE-PEG-Biotin as reported previously.[32-34] To detect B-MVs, we immobilize SA on the RGO-based FET biosensor channel surface via 1-pyrenebutanoic acid succinimidyl ester (PASE) as a cross-linking agent. Various concentrations of B-MVs are introduced to the sensing channel subsequently. Finally, electrical signal changes of the FET biosensor are recorded before and after the B-MVs-SA interaction. With the high and multivalent affinity of the streptavidin-biotin system as well as RGO as an excellent charge conducting material,

View Article Online
DOI: 10.1039/C9AN01332F

the detection of B-MVs with high sensitivity and specificity is realized. Moreover, our platform is capable of detecting B-MVs derived from different cell lines. In addition, the application of membrane biotinylation strategy makes this method universal to detect the entire MVs population. Therefore, the SA functionalized FET biosensor is hopeful to be a powerful tool for biomedical research.

2. Experimental section

2.1 Materials

1,2-distearoyl-sn-glycero-3-phosphoethanolamine-N-[biotinyl(polyethylene glycol)-2000)] (DSPE-PEG-Biotin) was ordered from Avanti Polar lipids, inc. (Alabaster, Alabama, USA). 1-pyrenebutanoic acid succinimidyl ester (PASE) was supplied by Sigma-Aldrich (Shanghai, China). Streptavidin (SA), cyanine-3 (Cy3), streptavidin-Cy3 (SA-Cy3) and 3,3′-dioctadecyloxacarbocyanine perchlorate (Dio) were supplied by Solarbio Science & Technology Co. Ltd. (Beijing, China). Bull serum albumin (BSA) was bought from Thalys Co. Ltd. (Wuhan, China). Graphite powders (99.99995%, 325 mesh) used in the experiments were bought from Alfa Aesar Co. Ltd. (Tianjin, China). Hydrazine (98%) was supplied by Aladdin Co. Ltd. (Shanghai, China). Anti-brain natriuretic peptide antibody (Anti-BNP antibody) was ordered from Abcam Co. Ltd. (Cambridge Science Park, UK). Anti-lipocalin-2 monoclonal antibody (Anti-LCN-2 monoclonal antibody) was purchased from Sigma-Aldrich (Shanghai, China). Equine-derived antibody against Ebola virus (EBOV) glycoprotein was provided by Wuhan Virus Research Institute of China. Human hpatocarcinoma cells (HepG2) and human umbilical vein endothelial cells (HUVEC) were obtained from American Type Culture Collection (ATCC, Manassas, VA, USA). The normal liver cell line HL-7702 was purchased from Procell Life

Science & Technology Co. Ltd. (Wuhan, China). Concentrated H_2SO_4, 35 wt % hydrogen peroxide (H_2O_2), phosphate buffer saline (PBS) and other chemical reagents were provided by Generay Biotech Co. Ltd. (Shanghai, China). Ultrapure water from Millipore water purification system (18.2 MΩ resistivity, Milli-Q Direct 8) was used throughout the research.

2.2 Fabrication of the RGO-based FET biosensor

Firstly, the FET device was fabricated as previously reported.[25] To construct source and drain electrodes, the photolithography and electron-beam evaporation were employed. Using the previously reported method, the standard RGO suspensions were obtained.[25,35] To fabricate the RGO-based FET device, the original RGO suspension was diluted to 0.2 mg/mL and was drop-casted onto the chip surface subsquently. By thermally annealling at 80°C for another 2 h, the contact between the RGO and the channel was further enhanced. Subsquently, the few-layer RGO-based FET biosensor was obtained by immersing the device in the Pirahna solution (7:3 v/v concentrated H_2SO_4/35 wt % H_2O_2) and further sonicating for 30 s. Finally, ultrapure water was applied to thoroughly wash the device and nitrogen was used to dry the device.

2.3 Immobilization of SA on the RGO surface

Firstly, PASE was used as a cross-linker to immobilize SA on the RGO surface. In practice, 5 mM PASE in dimethyl-sulfoxide (DMSO) was appiled to the RGO-based FET biosensor for 1 h at room temperature with foil wrapped to protect it from light. Afterwards, the biosensor was washed with pure DMSO, ethanol, and DI water, respectively. Then, SA (100 μg/mL) was introduced to the PASE-activated FET biosensor for another 2 h at room temperature. Finally, the SA-functionalized FET biosensor was rinsed with DI water for 3 times on the shaker to remove the excess SA probe. To prevent possible interference from nonspecific binding events, 1

mg/mL BSA solution was used and incubated with the SA-functionalized FET biosensor for 1 h. At last, the chip was rinsed by DI water for 3 times.

2.4 Cell Culture

Human liver cancer cells (HepG2), umbilical vein endothelial cells (HUVEC), normal liver cells (HL-7702), were routinely cultured in a 75 cm^2 culture flask (2×10^5 cells/cm^2) using RPMI-1640 complete cell culture medium (Cellgro) with/without 10 μg/mL DSPE-PEG-biotin, and incubated with 5% CO_2 at 37°C.

2.5 MVs and exosomes isolation

To achieve membrane biotinylation, RPMI-1640 complete cell culture medium supplemented with 10 μg/mL DSPE-PEG-Biotin was used to culture cells for 48 h. When the cells were grown to a confluence of 80%-90%, the cell medium was replaced with RPMI-1640 basal medium (supplemented with 10 μg/mL DSPE-PEG-Biotin) containing no fetal bovine serum (FBS) to culture the cells for another 48 h to stimulate vesicles releasing. After that, the cell medium was colleted and centrifuged at 300 g for 10 min and 2000 g for 20 min at 4°C to remove cells and cellular debris, respectively. To further diacard cellular debris, a 0.8 μm pore filter was appiled to filter the supernatant. Subsequently, the supernatant was centrifugated at 20, 000 g for 1 h at 4°C to obtain B-MVs sediment. For the purpose of purification, the sediment was further resuspended in sterile PBS, and centrifuged for another 1 h at 4°C at 20, 000 g. 200 μL of PBS was used to resuspend the pellet obtained. Finally, the purified B-MVs were stored in a -80°C refrigerator after dispensing.

Isolation of MVs from HepG2 cells without the addition of DSPE-PEG-biotin was carried out by using the same method.

Exosomes were isolated from cell culture supernatant using the similar centrifugation process. After the same steps mentioned above to discard cellular debris, a 0.22 μm pore filter was used to filter the supernatant. Subsequently, the sediment was further centrifuged at 10, 000 g for 30 min to remove large vesicles, such as MVs and protein aggregatest, and 110, 000 g for 70 min to acquire exosome sediment at 4°C. For exosomes purification, the sediment was further resuspended in sterile PBS, and centrifuged at 110, 000 g at 4°C for another 70 min. Finally, 200 μL of PBS was used to resuspend the pellet obtained. At last, the purified exosomes were stored in a -80°C refrigerator after dispensing.

2.6 Characterization of B-MVs

TEM: Transmission electron microscopy (TEM, Hitachi H-7000 NAR) operated at 80 kV was appiled to characterize both morphology and size of the as-prepared HepG2-derived B-MVs. Briefly, 10 μL of diluted B-MVs pellet was first dropped onto a carbon-coated film copper grid with 2% glutaraldehyde (Sigma-Aldrich). Then, 2% phosphotungstic acid (Sigma-Aldrich) were placed onto the grids, followed by rinsing with PBS and dried at room temperature for subsequent TEM observation.

NTA: The particle size distribution, concentration and zeta potential of the B-MVs were characterized by a nanoparticle tracking analysis device (NTA, Zeta view Ltd., Germany). Before introducing into the device, a 0.8 μm pore filter was employed to filtrate 50 μL of diluted B-MVs pellets. Subsequently, the Brownian motion of B-MVs could be recorded by the camera and the hydrodynamic diameter and concentration of the nanoparticles could be calculated using the Stockes-Einstein equation under optimized condition finally. Each sample was tested 3 times under room temperature.

View Article Online
DOI: 10.1039/C9AN01332F

SEM: Scanning electron microscopy (SEM) (Zeiss, Germany) was applied to characterize RGO deposited onto the channel surface and B-MVs captured on the chip surface. To observe RGO deposited onto the channel surface, the RGO suspension (0.2 mg/mL) was drop-casted onto the channel surface and the device was further sonicated for 30 s in the Pirahna solution for the final SEM analysis. For B-MVs observation, B-MVs captured on the FET channel surface were firstly fixed with 2.5% glutaraldehyde overnight at room temperature. Subsequently, the samples were gradient dehydrated using ethanol solution. At last, the prepared samples were further sputtered with platinum nanoparticles (10 nm) for 60 s for the final SEM imaging.

Fluorescence colocalization analysis: A fluorescence microscope Olympus DP72 (Olympus, Japan) was used to characterize the successful biotinylation of MVs by fluorescence colocalization analysis. 10 μL of B-MVs resuspended in 1×PBS were added to SA-Cy3 (1mg/mL) at 1:200 dilution incubated for 1 h at room temperature. Then, the mixture was further added to Dio (10mg/mL) at 1:300 dilution. 10 μL of MVs (without addition of DSPE-PEG-biotin) were stained using the same protocol mentioned above. At last, the fluorescence microscope was used to capture the fluorescence images of B-MVs and MVs derived from HepG2 cells.

Flow cytometry analysis of biotinylation efficiency of HepG2 cells and B-MVs: To ensure the high biotinylation efficiency of MVs for subsequent FET detection, the biotinylation efficiency of mother cells (HepG2 cells) was tested firstly. 10 μL of biotinylated HepG2 and HepG2 cells (without addition of DSPE-PEG-biotin) re-suspended in 1×PBS were added to SA-Cy3 (1 mg/mL) at 1:200 dilution and incubated for 1 h at room temperature. Then, flow cytometry was used to detect the biotinylation efficiency of HepG2 cells. Meanwhile, the biotinylation efficiency of MVs derived from biotinylated HepG2 cells and HepG2 cells was tested using the

similar protocol mentioned above. All flow cytometry results were analyzed by FlowJo software.

2.7 Electrical measurements

A semiconductor parameter analyzer (Keithley 4200-SCS) coupled with a probe station (EverBeing BD-6) was used for all the electrical measurements. With a Ag/AgCl reference electrode used as a solution-gate electrode, all the electrical measurements of the RGO-based FET biosensor were conducted by immersing Ag/AgCl reference electrode in 0.01×PBS. 10 μL of 0.01×PBS and 10 μL of B-MVs samples were applied onto the biosensor channel for blank control and target analysis, respectively. A constant bias V_{ds}=0.1 V (the drain-source voltage) for all electrical test was applied.

3. Results and discussion

3.1 Working principle

Fig. S1 demonstrates the fabrication process and working principle of the SA-functionalized FET biosensor for detection of B-MVs. First of all, the FET chip is fabricated on a SiO_2/Si substrate by appling the traditional standard semiconductor technology. Afterwards, the RGO-based FET biosensor is obtained by dropping-casting the RGO as the conducting material onto the channel surface. As shown in the Fig. S2, we could clearly see the RGO wrinkles spanned across the source and drain electrode, indicating that RGO has been successfully deposited onto the channel surface and the sensing channel has been connected as anticipated. Then, PASE is modified onto the RGO surface as a crosslinker molecule through π-π interaction between RGO surface and the pyrene group on PASE. Through the

View Article Online
DOI: 10.1039/C9AN01332F

covalent bonding between another amide bond on PASE and an amino group on SA, the capture probe SA is decorated onto the RGO surface subsequently. To prevent possible interference caused by nonspecific adsorption, BSA is employed after SA functionlization. Prior to detection, MVs are biotinylated via a membrane biotinylation strategy. Finally, the SA probe is specifically reacted with B-MVs, which are applied to the surface of the chip. The electrical signal change (the Dirac point change of I_{ds}-V_g curves of the RGO-based FET biosensor) before and after the reaction is monitored by using a silver wire as the gate electrode.

3.2 Characterization of B-MVs

B-MVs were firstly purified from different cell culture supernatant by using differential ultracentrifugation method with slight modifications as reported previously.[22,32] In order to characterize the as-prepared B-MVs, TEM and NTA were then used to reflect morphology, particle size distribution, concentration and zeta potential of B-MVs. The TEM image in Fig. 2a shows that the typical B-MVs with membranous structure were cup-shaped and heterogeneous in size, with the particle size ranging from about 100 to 500 nm, which is consistent with the basic characteristics of MVs in other reported works.[36,37] Fig. 2b presents that the isolated B-MVs with a diameter of ~207 nm were larger and more heterogeneous than exosomes, and the original concentration of B-MVs was 1.9×10^9 particles/mL. Moreover, the proportion of B-MVs above 100 nm was greater than 95% after high-speed centrifugation pretreatment, indicating the successful B-MVs isolation. This size distribution result is consistent with that reported in the previous literatures.[22,38-40] Moreover, as shown in Fig. S3, the zeta potential of B-MVs was -18.4 mV, indicating that B-MVs are negatively charged.

To characterize the successful biotinylation of MVs, flow cytometry and fluorescence colocation analysis were employed. In practice, we first evaluated the biotinylation efficiency of HepG2 cells (the parent cell of B-MVs) by incubating biotinylated HepG2 cells and HepG2 cells (as a control) with SA-Cy3 for 1 h at room temperature. As illustrated in Fig. 2c, HepG2 cells were successfully biotinylated with an excellent efficiency of 99.5% compared to the control HepG2 cells (without biotinylation), indicating that HepG2 cells had been nearly all biotinylated. This superior biotinylation effiency of HepG2 cells was consistent with other reported results.[33] At last, the biotinylation effiency of MVs derived from biotinylated HepG2 cells was obtained by incubating B-MVs (with biotinylation) and MVs (without biotinylation) with SA-Cy3 for 1 h at room temperature. As shown in Fig. 2d, MVs released from biotinylated HepG2 cells have been effectively biotinylated with an efficiency of 92.6% compared to the control MVs. This result denoted that the vast majority of MVs had been successfully biotinylated as anticipated. The excellent biotinylation effiency of MVs also corresponded to other reports in the literatures.[32,33] Moreover, the fluorescence colocation analysis was carried out by using the similar method reported by other work.[33] Moreover, the results in Fig. S4 indicate that the SA-Cy3 labeled B-MVs (red fluorescence) showed an apparent colocalization with the DiO-labeled B-MVs (green fluorescence). However, this phenomenon was not seen in MVs (as a control), suggesting the absense of biotin on the surface of MVs. These results indicate that MVs have been successfully biotinylated via a membrane biotinylation strategy. High-efficiency biotinylation of MVs provides a reliable basis for subsequent FET biosensor detection of B-MVs based on biotin-streptavidin high-affinity binding systems. In conclusion, all these above results demonstrate that the B-MVs have been successfully obtained.

View Article Online
DOI: 10.1039/C9AN01332F

3.3 Verification of successful SA modification

In order to confirm the successful functionalization of SA probe on the RGO surface, SA-Cy3 and Cy3 (as a control) were respectively dropped to the silicon surface which was already activated by PASE. The successful modification of SA on chip surface was verified by fluorescence microscope. As shown in Fig. 3a, an apparent red fluorescence was observed when SA-Cy3 was applied to PASE-modified silicon surface. However, when Cy3 was introduced to the PASE-modified silicon surface, we could only see negligible fluorescence from the image in Fig. 3b.

In addition, the transfer curves of the RGO-based FET were recorded before and after the SA immobilization to further verify the successful functionalization of SA probe on the device surface. In Fig. 3c, the ambipolar properties of RGO could be clearly observed from the "U"-shaped black curve. Because of the p-doping of PASE, the red curve obtained after PASE modification shifted to right subsquently. This phenomenon is consistent with the other reported work.[41] Moreover, the light blue curve shifted to the left after the immobilization of the SA probe because of the n-doping of SA (pI=6.0, negative charged in 1×PBS). These results show that probe SA has been successfully modified on the surface of the chip as expected.

3.4 Feasibility of the detection principle

To confirm the feasibility of detection principle, a relatively low concentration of B-MVs (10^5 particles/mL, 10μL) were introduced onto the SA-functionalized FET biosensor subsquently. As illustrated in Fig. 3c, the green curve greatly shifted to left after introducing B-MVs onto the SA-functionalized FET biosensor channel because of the n-doping of B-MVs. This phenomenon illustrates that the detection principle is feasible and our as-fabricated FET biosensor is very sensitive to B-MVs.

To further intuitively demonstrate the feasibility of the detection principle, we used SEM to visualize the B-MVs captured by the SA probe modified on the FET biosensor. In Fig. 3d, we could clearly see that B-MVs were successfully captured in the sensing channel of the FET biosensor with a typical MVs structure.[42] Moreover, these visible B-MVs had a particle diameter of about 200-300 nm, which was consistent with our results mentioned above in Fig. 2b. This result further proves that the developed SA-functionalized FET biosensor has the capability to capture B-MVs and our detection principle is feasible.

3.5 Sensitivity

By introducing increasing concentrations of the previously prepared B-MVs standard solutions (10^4 particles/mL-10^9 particles/mL) to the SA-functionalized FET biosensor, the sensitivity of the RGO-based FET biosensor for B-MVs detection was investigated. The corresponding transfer characteristic curves were recorded in Fig. 4. To monitor the response of the RGO-based FET biosensor upon addition of B-MVs at various concentrations, the V_{CNP} (charge neutral point, namely, the lowest point of the transfer curve) was used. With increasing concentrations of the B-MVs from 10^4 particles/mL to 10^9 particles/mL adding to the FET biosensor, the V_{CNP} of the devices kept moving to the left, which was shown in Fig. 4a. This phenomenon is mainly due to the continuous accumulation of negative charge on the graphene surface with the addition of increasing concentration of B-MVs, which eventually led to a continuous n-type doping of graphene. The biosensor response to B-MVs was quantified using the change of V_{CNP} ($\Delta V_{CNP,}$ namely, the amount of change in V_{CNP} relative to SA after reaction with different concentrations of B-MVs). Fig. 4b shows the relationship between ΔV_{CNP} versus different concentrations of B-MVs. As we can see, the lgC which is the logarithmic value of B-MVs concentration shows a good linear response

to the $-\Delta V_{CNP}$. The linear relationship could be expressed as $-\Delta V_{CNP}=34.6\lg C_{B\text{-}MVs}-131.1$ ($R^2=0.99$). The 3 fold noise level (~18mV) could be obtained by using 0.01×PBS as blank control, which is represented by the black dashed line in Fig. 4b. Subsequently, the detection limit (LOD) of 20 particles/μL could be calculated with a signal 3 times more than the background with the formula mentioned above. Cherré et al.[22] reported the specific detection of $CD31^+$ MVs derived from endothelial cell through anti-CD31 antibody immobilized magnetoresistive biosensor with LOD lowerd to 1×10^5 particles/μL. Kailashiya et al.[23] reported the successful detection of MVs by the electrochemical biosensor with a LOD of 10^2 particles/μL, in which the anti-PAC1 antibody was modified on the electrode surface. Singh et al.[24] also fabricated an anti-PAC1 and anti-P-selectin antibodies functionlized electrochemical biosensor for MVs detection with a LOD lowered to 96 particles/μL. The performance comparison of various MVs biosensors was summurized in Table S1. Obviously, the proposed RGO-based FET biosensor shows the lowest detection limit (20 particles/μL), which is probably caused by the usage of RGO as an excellent charge conducting material and SA as a capture probe to monitor $B\text{-}MV_S$ in a 1:4 recognition format.

3.6 Specificity

To study the specificity of the FET biosensor, HepG2-derived B-MVs, MVs, and exosomes, respectively, were introduced to the SA-functionalized FET devices. 0.01×PBS instead of target B-MVs was conducted for noise level test. Fig. S5 shows the transfer curves of the SA-functionalized RGO-FET biosensor incubated with 0.01×PBS, MVs (10^9 particles/mL), exosomes (10^9 particles/mL) and B-MVs (10^5 particles/mL), respectively. Obviously, the shift of V_{CNP} ($|\Delta V_{CNP}|$) of the B-MVs was much larger, while the $|\Delta V_{CNP}|$ of other interferences were observed to be negligible.

As demonstrated in Fig. 5a, the $|\Delta V_{CNP}|$ versus B-MVs and the interferences are summarized. The $|\Delta V_{CNP}|$ of MVs, exosomes and 0.01×PBS were about 2.33, 4.67, 3.33, respectively. These signal responses are probably caused by the nonspecific adsorption. However, the $|\Delta V_{CNP}|$ of B-MVs was found to be approximately 34, which is more than 7 fold of that of other substances.

To further verify the specificity of the biosensor for detecting B-MVs, different antibodies on the surface of the chip including anti-LCN-2, anti-EBOV, anti-BNP, respectively, were modified instead of SA. The results in Fig. 5b show that only the chip modified with SA had a significant response to B-MVs, while the signals of other probes were almost negligible. $|\Delta V_{CNP}|$ were about 6.67, 9.33, 6 when chips are modified with anti-LCN-2, anti-EBOV, anti-BNP antibodies, respectively. However, $|\Delta V_{CNP}|$ of SA was found to be approximately 75.33, which is more than 8 fold of that of other antibodies. Excellent specificity of RGO-based FET biosensor is clearly indicated by the above results.

3.7 Versatility

In order to verify the versatility of our designed platform, various B-MVs derived from different cell origins (e.g., hepatoma cells HepG2, HUVEC cells and normal liver cells HL-7702) were prepared, then the SA-functionalized RGO FET chip was reacted with the as-prepared B-MVs. As shown in Fig. 6, various B-MVs derived from different cell lines were successfully detected using our unique platform, and $|\Delta V_{CNP}|$ of biotinylated HepG2 derived-, HUVEC derived- and HL-7702 derived-MVs were approximately 192, 159, and 128, respectively. Apparently, the B-MVs derived from hepatoma cells had a maximum response compared to the other two groups, indicating that MVs have a high pathological concentration in hepatocellular carcinoma by correlating the FET signals with the concentration of

View Article Online
DOI: 10.1039/C9AN01332F

MVs using the equation mentioned above in Fig. 4b. Statistically, there were significant differences between HepG2 cells group and HL-7702 cells group ($P<0.01$), HepG2 cells group and HUVEC cells group ($P<0.05$), respectively. The results are consistent with those reported by the other literature.[15] The increased level of circulating MVs in hepatocellular carcinoma patients is attributed to the enhanced formation and/or decreased clearance of MVs as reported previously.[43] What's more, the different responses of the control cell groups are contributed to intrinsic divergence to secrete MVs between different cell lines probably. Therefore, the FET biosensor we designed to detect B-MVs is universal and we unveil that there is a significant difference in the concentration of B-MVs derived from cancer cells and normal cells by appling our platform.

4. Conclusions

In summary, a SA-functionalized FET biosensor capable of detecting B-MVs with high sensitivity, specificity and versatility by utilization of a membrane biotinylation strategy has been successfully developed. Such an unique platform holds tremendous advantages, such as, i) the application of the membrane biotinylation strategy to engineer the MVs with a highly expressed "biomarker" (biotin) coupled with SA as the capture probe in a 1:4 recognition format, thus lowering the detection limit to 20 particles/μL, ii) the utilization of graphene-based FET biosensor, therefore realizing highly sensitive B-MVs detection,. iii) more importantly, this approach also allows for monitoring B-MVs derived from different cells lines, suggesting its versatility for B-MVs detection. All of these advantages indicate that this work provides a completely new strategy for entire MVs population analysis in biomedical research.

View Article Online
DOI: 10.1039/C9AN01332F

Conflicts of interest

There are no conflicts to declare.

Acknowledgements

This work was supported by the National Natural Science Foundation of China (No. 21675041)

Supporting Information

Supplementary data associated with this article can be found in the online version at …

View Article Online
DOI: 10.1039/C9AN01332F

References

1 H. Kalra, G. Drummen and S. Mathivanan, *Int. J.Mol. Sci*, 2016, **17**, 170.

2 G. Raposo and W. Stoorvogel, *J. Cell Biol*, 2013, **200**, 373-383.

3 M. Tkach and C. Thery, *Cell*, 2016, **164**, 1226-1232.

4 M. Yanez-Mo, P. R. Siljander, Z. Andreu, A. B. Zavec, F. E. Borras, E. I. Buzas, K. Buzas, E. Casal, F. Cappello and J. Carvalho, *J. Extracell. Vesicles*, 2015, **4**, 27066.

5 D. Burger, S. Schock, C. S. Thompson, A. C. Montezano, A. M. Hakim and R. M. Touyz, *Clin. Sci*, 2013, **124**, 423-441.

6 J. Ratajczak, M. Wysoczynski and F. Hayek, *Leukemia*, 2006, **20**, 1487.

7 A. E. Sedgwick and C. D'Souza-Schorey, *Traffic*, 2018, **19**, 319-327.

8 I. D. Conde, C. N. Shrimpton and P. Thiagarajan, *Blood*, 2005, **106**, 1604-1611.

9 M. L. Liu and K. J. Williams, *Curr. Opin. Endocrinol*, 2012, **19**, 121-127.

10 J. Perez-Hernandez and R. Cortes, *Dis. Markers*, 2015, **2015**, 613536.

11 E. Colombo, B. Borgiani, C. Verderio and R. Furlan, *Front Physiol*, 2012, **3**, 63.

12 C. D 'Souza-Schorey and J. W. Clancy, *Genes Dev*, 2012, **26**, 1287-1299.

13 I. Giusti, S. D'Ascenzo and V. Dolo, *Biomed. Res. Int*, 2013, **2013**, 703048.

14 J. G. Ren, Q. W. Man and W. Zhang, *J Dent Res*, 2016, **95**, 87-93.

15 W. Wang, H. Li, Y. Zhou and S. Jie, *Cancer Biomark*, 2013, **13**, 351-357.

16 J. Baran, M. Baj-Krzyworzeka and K. Weglarczyk, *Cancer Immunol Immun*, 2010, **59**, 841-850.

17 R. A. Dragovic, C. Gardiner, A. S. Brooks, D. S. Tannetta, D. J. P. Ferguson, P. Hole, B. Carr, C. W. G. Redman, A. L. Harris and P. J. Dobson,

View Article Online
DOI: 10.1039/C9AN01332F

Nanomed.-Nanotechnol.Biol.Med, 2011, **7**, 780-788.

18 A. S. Lawrie, A. Albanyan, R. A. Cardigan, I. J. Mackie and P. Harrison, *Vox Sang*, 2009, **96**, 206-212.

19 S. L. Maas, J. De Vrij, E. J. Van der Vlist, B. Geragousian, L. Van Bloois, E. Mastrobattista, R. M. Schiffelers, M. H. Wauben, M. L. Broekman and E. N. Nolte-'t Hoen, *J. Control. Release*, 2015, **200**, 87-96.

20 M. S. Chiriaco, M. Bianco, A. Nigro, E. Primiceri, F. Ferrara, A. Romano, A. Quattrini, R. Furlan, V. Arima and G. Maruccio, *Sensors-Basel*, 2018, **18**, 3175.

21 S. Chaudhuri, T. Korten, S. Korten, G. Milani, T. Lana, G. Te Kronnie and S. Diez, *Nano Lett*, 2018, **18**, 117-123.

22 S. Cherré, E. Fernandes, J. Germano, T. Dias, T. Cardoso, M. S. Piedade, N. Rozlosnik, M. I. Oliveira and P. P. Freitas, *Analyst*, 2017, **142**, 979-986.

23 J. Kailashiya, N. Singh and S. K. Singh, *Biosens. Bioelectron*., 2015, **65**, 274-280.

24 P. Singh, S. Srivastava and P. Chakrabarti, *Sensor Actuat B-Chem*, 2017, **240**, 322-329.

25 B. J. Cai, S. T. Wang, L. Huang, Y. Ning, Z. Y. Zhang and G. J. Zhang, *ACS Nano*., 2014, **8**, 2632-2638.

26 B. J. Cai, L. Huang, H. Zhang, Z. Y. Sun, Z. Y. Zhang and G. J. Zhang, *Biosens. Bioelectron*., 2015, **74**, 329-334.

27 C. Zheng, L. Huang, H. Zhang, Z. Y. Sun, Z. Y. Zhang and G. J. Zhang, *ACS Appl. Mater. Interfaces*., 2015, **7**, 16953-16959.

28 J. C. Mei, Y. T. Li, H. Zhang, M. M. Xiao, Y. Ning, Z. Y. Zhang and G. J. Zhang,

View Article Online
DOI: 10.1039/C9AN01332F

Biosens. Bioelectron., 2018, **110**, 71-77.

29 Y. M. Lei, M. M. Xiao, Y. T. Li, L. Xu, H. Zhang, Z. Y. Zhang and G. J. Zhang, *Biosens. Bioelectron*., 2017, **91**, 1-7.

30 C. Zhang, J. Q. Xu, Y. T. Li, L. Huang, D. W. Pang, Y. Ning, W. H. Huang, Z. Y. Zhang and G. J. Zhang, *Anal. Chem*., 2016, **88**, 4048-4054.

31 H. Xie, Y. T. Li, Y. M. Lei, Y. L. Liu, M. M. Xiao, C. Gao, D. W. Pang, W. H. Huang, Z. Y. Zhang and G. J. Zhang, *Anal. Chem*., 2016, **88**, 11115-11122.

32 G. Chen, J. Y. Zhu, Z. L. Zhang, W. Zhang, J. G. Ren, M. Wu, Z. Y. Hong, C. Lv, D. W. Pang and Y. F. Zhao, *Angew. Chem. Int. Edit*, 2015, **54**, 1036-1040.

33 W. Zhang, Z. L. Yu, M. Wu, J. G. Ren, H. F. Xia, G. L. Sa, J. Y. Zhu, D. W. Pang, Y. F. Zhao and G. Chen, *ACS Nano*., 2017, **11**, 277-290.

34 L. Zhu, D. Dong, Z. L. Yu, Y. F. Zhao, D. W. Pang and Z. L. Zhang, *ACS Appl. Mater. Interfaces*., 2017, **9**, 5100-5108.

35 V. C. Tung, M. J. Allen, Y. Yang and R. B. Kaner, *Nat. Nanotechnol*, 2009, **4**, 25-29.

36 E. Van Der Pol, A. G. Hoekstra, A. Sturk, C. OTTO, T. G. VAN LEEUWEN and R. NIEUWLAND, *J. Thromb. Haemost*, 2010, **8**, 2596-2607.

37 Y. G. Zhou, R. M. Mohamadi, M. Poudineh, L. Kermanshah, S. Ahmed, T. S. Safaei, J. Stojcic, R. K. Nam, E. H. Sargent and S. O. Kelley, *Small*, 2016, **12**, 727-732.

38 E. Cocucci, G. Racchetti and J. Meldolesi, *Trends Cell Biol*, 2009, **19**, 43-51.

39 B. György, K. Módos and É. Pállinger, *Blood*, 2011, **117**, e39-e48.

40 M. N. Munkonda, S. Akbari and C. Landry, *J. Extracell. Vesicles*, 2018, **7**, 1432206.

41 Z. Hao, Y. Zhu, X. Wang, P. G. Rotti, C. DiMarco, S. R. Tyler, X. Zhao, J. F. Engelhardt, J. Hone and Q. Lin, *ACS Appl. Mater. Interfaces*., 2017, **9**, 27504-27511.

42 B. A. Mrvar, V. Šuštar and V. Janša, *Blood. Cell. Mol. Dis*, 2010, **44**, 307-312.

43 S. Lemoinne, D. Thabut, C. Housset, R. Moreau, D. Valla, C. M. Boulanger and P. E. Rautou, *Nat. Rev. Gastro. Hepat*, 2014, **11**, 350-361.

View Article Online
DOI: 10.1039/C9AN01332F

Figure captions

Fig. 1. Schematic diagram of the SA-functionalized FET biosensor for detection of B-MVs released from cultivated cells via a membrane biotinylation strategy.

Fig. 2. Characterization of B-MVs. (a) Transmission electron microscopy image of typical B-MVs derived from HepG2 cell. Scale bars, 1 μm. (b) The particle distribution and concentration of B-MVs derived from HepG2 cell analyzed by nanoparticle tracking analyzer. (c) Biotinylation efficiency of HepG2 cells by flow cytometry analysis. Red histogram shows fluorescence of SA-Cy3 incubated with HepG2 cells (as a control), blue histogram shows fluorescence of SA-Cy3 incubated with biotinylated HepG2 cells. (d) Biotinylation efficiency of B-MVs by flow cytometry analysis. Red histogram shows fluorescence of SA-Cy3 incubated with MVs, blue histogram shows fluorescence of SA-Cy3 incubated with B-MVs.

Fig. 3. The fluorescence microscope image of a silicon chip modified with (a) SA-Cy3 and (b) Cy3 with PASE as crosslinker molecule. Scale bars, 100 μm. (c) The transfer curves of the RGO-based FET modified with PASE, immobilized with SA probe and reacted with B-MVs (10^5 particles/mL). (d) Scanning electron microscope image of B-MVs captured on the surface of the FET biosensor channel. Scale bars, 200 nm.

Fig. 4. (a) Transfer characteristics and (b) shift of V_{CNP} of the SA-immobilized RGO-based FET biosensors treated with the B-MVs at a series of concentrations (10^4 particles/mL-10^9 particles/mL). Dashed line represents the 3 fold noise level (~18 mV) from the blank control test. Error bars represent standard deviations of measurements (n=3).

Fig. 5. (a) The shift of V_{CNP} of the SA-immobilized RGO-based FET biosensors incubated with 0.01×PBS, 10^9 particles/mL MVs, 10^9 particles/mL exosomes, and 10^5

particles/mL B-MVs. (b) The shift of V_{CNP} of the different probe (anti-LCN-2, anti-EBOV, anti-BNP, SA) immobilized RGO-based FET biosensors incubated with 0.01×PBS and 10^6 particles/mL HepG2-derived B-MVs. Error bars represent standard deviations of measurements (n=3).

Fig. 6. The shift of V_{CNP} of the SA-immobilized FET biosensors for detecting B-MVs derived from HUVEC, HL-7702 and HepG2 cells, respectively. Error bars represent standard deviations of measurements (n=3). Differences between B-MVs derived from different cells were statistically significant (Welch t-test). **: $p< 0.01$, *: $p<0.05$.

View Article Online
DOI: 10.1039/C9AN01332F

Fig. 1.

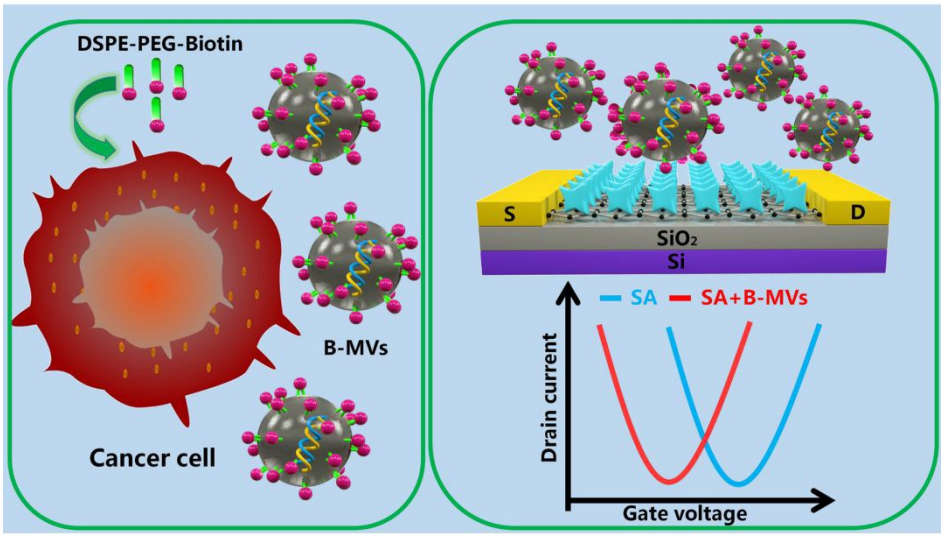

View Article Online
DOI: 10.1039/C9AN01332F

Fig. 2.

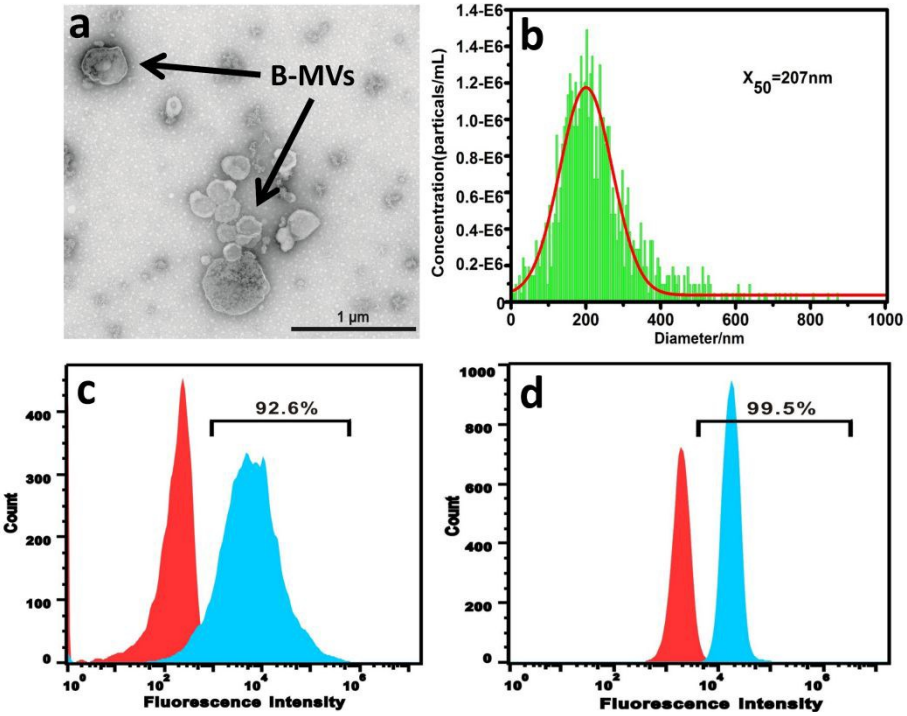

View Article Online
DOI: 10.1039/C9AN01332F

Fig. 3.

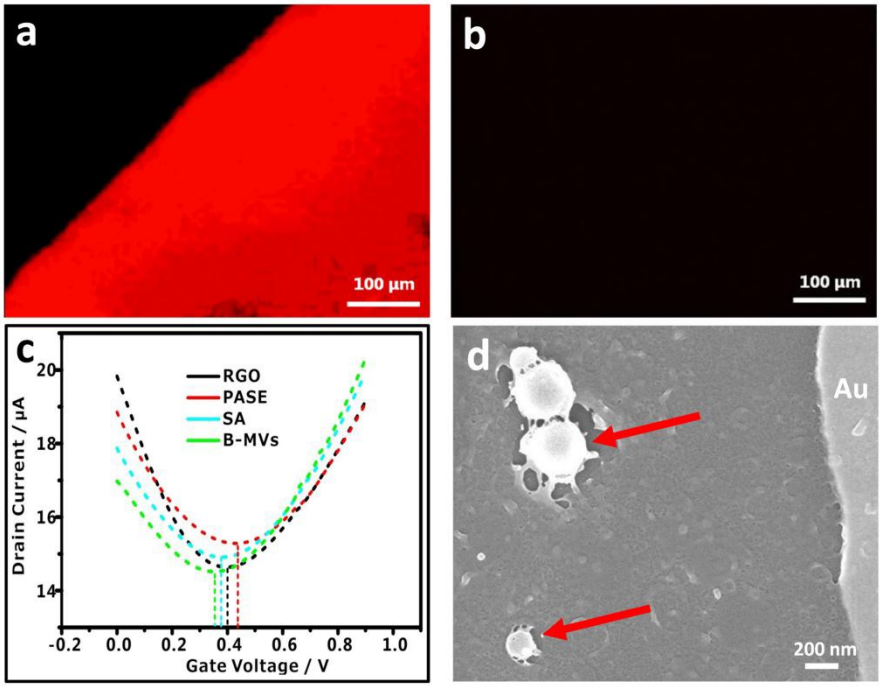

View Article Online
DOI: 10.1039/C9AN01332F

Fig. 4.

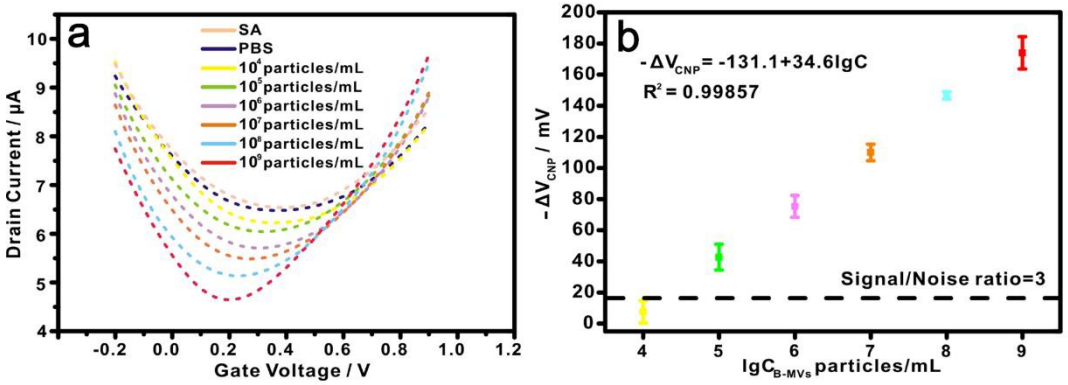

View Article Online
DOI: 10.1039/C9AN01332F

Fig. 5.

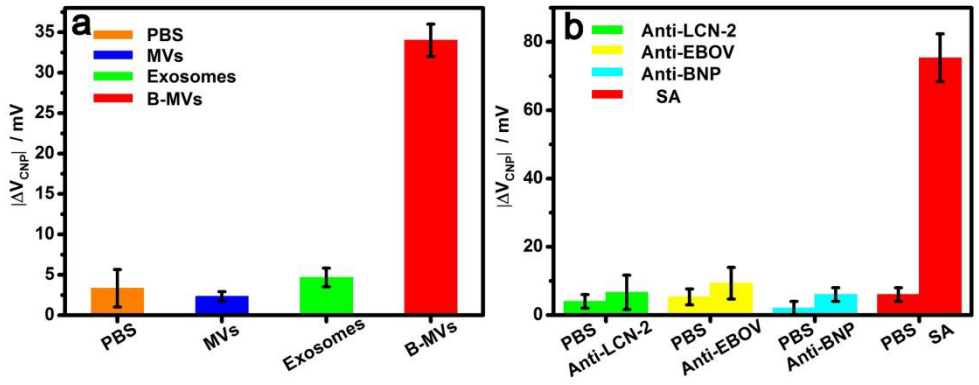

View Article Online
DOI: 10.1039/C9AN01332F

Fig. 6.

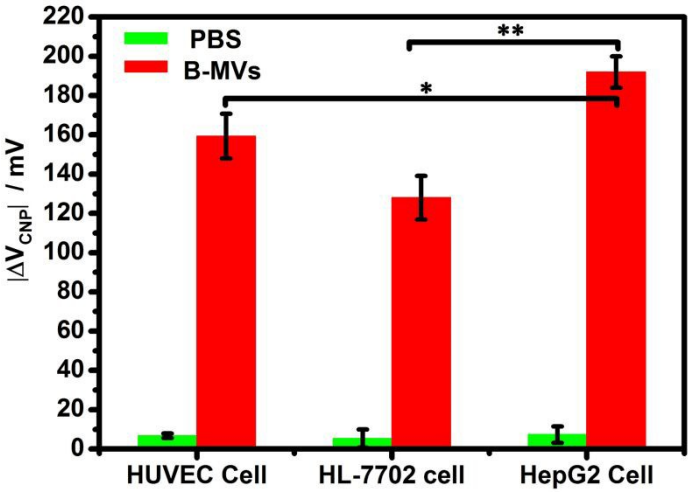

View Article Online
DOI: 10.1039/C9AN01332F

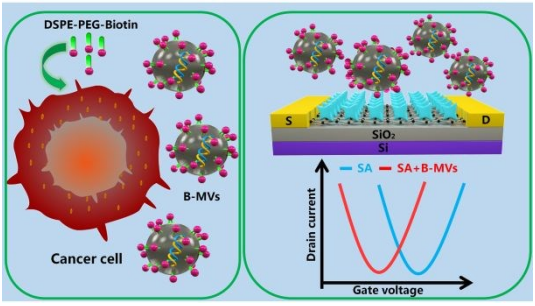

Highlights:

A Reduced Graphene Oxide Field Effect Transistor Biosensor for Detection of Microvesicles by Using a Membrane Biotinylation Strategy.